

Centralized and Decentralized Optimal Control of Single Speed Heat Pumps

Ryan S. Montrose, John F. Gardner, Aykut C. Satici

Department of Mechanical & Biomedical Engineering

Boise State University

1910 W. University Drive, Boise, ID 83706

Abstract

Whether naturally occurring or in response to a demand event, utility service providers are often challenged with aggregated load synchronization. This synchronization can cause damage to various grid sub-systems further compounding the issue. The contribution of this paper is the development of an optimal decentralized control algorithm for commonly used single speed heat pumps. Our control architecture allows for the regulation of home temperatures while simultaneously minimizing the aggregate load volatility and peak power consumption by means of peer to peer communication. An optimal centralized controller is also explored and compared against its decentralized counterpart.

Keywords: Optimal Control, Decentralized control, Adaptive control, Parameter estimation, Demand response, Thermostatically controlled load

Nomenclature

Indices

H Time horizon

i^k Horizon time step

K Simulation Horizon

k Time step

p Home number

State Information

m_p^k Control input of the p^{th} home at the k^{th} time step

T_p^k Temperature of the p^{th} home at the k^{th} time step

Other Symbols

Δt Step length

1. Introduction

The target of a 100% renewable electric supply system presents significant challenges to the organizations responsible for maintaining the reliability and resilience

of electric grids. While grid-level battery storage is often touted as the solution to integrating high penetrations of variable generating resources [1] [2] (e.g. solar PV and wind generators), there is a growing body of research pointing to the potential for flexibility and control of demand to play a significant role in grid operations going forward. In this regard, thermostatically controlled loads (TCLs) are some of the most sensible areas to explore because they make up a significant portion of demand on any given electric grid and there is a great deal of flexibility when they actually draw power [3].

To realize the true potential of TCLs as a resource to aid in grid operations, it is widely understood that numerous loads must be aggregated and controlled in a coordinated fashion. Many researchers have proposed methods of centralized control of aggregated TCLs and the problem of synchronization often arises [4]. The most common example of synchronization occurs during load-shedding demand response events. Many utilities have programs in which homeowners agree to allow the grid operators to occasionally turn off their air conditioning compressor in return for a rebate or reduction in rates. When the grid operator anticipates that they will have a difficult time meeting load requests, then many compressors can be shut off, thus shedding that load. The problem arises when the demand response event

is released. At this point a large portion of the compressors will cycle on because the building's temperature has no doubt risen in temperature during the demand response event. This often results in an immediate peak that is higher than the peak they were attempting to avoid. Subsequently, a period of oscillations occurs, during which time the aggregate load experiences large oscillations.

This paper explores innovative approaches to controlling an aggregation of TCLs by applying a combination of optimum control theory and localized communication between individual TCL's which serve to prevent inadvertent synchronization while minimizing peak demand.

The work presented in this paper builds on the body of research dedicated to smart grid systems. A smart grid system, defined by its ability to efficiently balance various energy streams, has been shown to increase both stability and efficiency of electric grids. Due to the vastness of smart grid applications, it's often helpful to define a smart grid by its constitutive subcategories. These categories include, but are not limited to, demand response events, agent based modeling, dynamic price control, and thermostatically controlled loads (TCLs).

Much of the body of literature in demand response and TCLs stems from Malhamé and Chong's seminal paper [5]. This paper introduced a stochastic control framework designed to aggregate a large population of homogeneous TCLs (electric space heaters) that are modeled with a pair of coupled Focker Plank equations (CFPEs). Two decades later, Callaway [6] built upon Malhamé and Chong's work not only by deriving an exact solution to the CFPEs, but also devised a method to aggregate TCLs about the variably-produced renewable energy sources.

As the field of smart grid systems matured, so too followed unique control methods designed to regulate aggregate power consumption. As it pertains to TCLs, two primary classifications exist: centralized and decentralized control. Various centralized control approaches are utilized to aggregate TCLs. For instance, various state-bin transition techniques are proposed in [7, 8, 9]. These binning techniques stochastically characterize the flow of TCLs between their respective off and on states. Through the systematic transitioning of states, an aggregate power reference signal is thereby tracked. Amongst [8, 9], including [10, 11], a model predictive control framework is used to optimally schedule a population of control actions. Machine learning techniques have also been adopted into the control of smart grid systems. In [12, 13, 14], a reinforcement learning control framework is used to learn the complex action space of

a population of TCLs. Other notable approaches to the aggregation of TCLs are the priority-stack-based controllers presented in [1], [15], and the unique geometric approach proposed in [10]. Lastly, several publications have been dedicated to the reduction aggregate power consumption via dynamic price control [16], [17].

Another classifier for TCLs, under the umbrella of smart grid systems, is decentralized control. In terms of large scale aggregation of TCLs, a centralized command structure is inherently burdened with the computation and communication complexities associated with its operation. Both scalability and cyber-security are often cited as the primary concerns of a centralized network topology when governing the actions of TCLs [18], [19]. Of the literature results in decentralized control, like that of the stochastic framework proposed in [20], methods of distributing the computational complexity to its participating patrons is explored. In both [21] and [22], decentralized controllers have been shown to resist various cyber-attacks and communication failures caused by network dropout.

The rest of this paper is organized as follows. In Section 2 a second order equivalent thermal parameter model of a TCL is presented along with its state space representation. A parameter estimation method is presented thereafter using the recursive least squares algorithm. Lastly, justifications for the network architecture and demand response event is provided. In Section 3 an optimization program is provided for both the decentralized and centralized control frameworks. Simulation results are presented Section 4 followed by closing remarks made in Section 5.

2. Background

Thermostatically controlled loads (TLCs), such as water heaters and HVAC systems, constitute the majority of power consumption in a typical residential setting. Through the proper control of such devices, a substantial portion of this energy may be saved and/or deferred. This paper focuses on the causal relationship between a population of single speed heat pumps (SSHPs) and the aggregate power consumption through an intermediary decentralized controller. Development of this decentralized controller begins by defining a thermal model which describes the temperature evolution of a residential home. In particular, this decentralized controller employs the well established second-order equivalent thermal parameter (ETP) model [7]. A second-order ETP model, like the one shown in Figure 1, describes the coupled relationship between the fast changing indoor air temperature and the slower bulk mass temper-

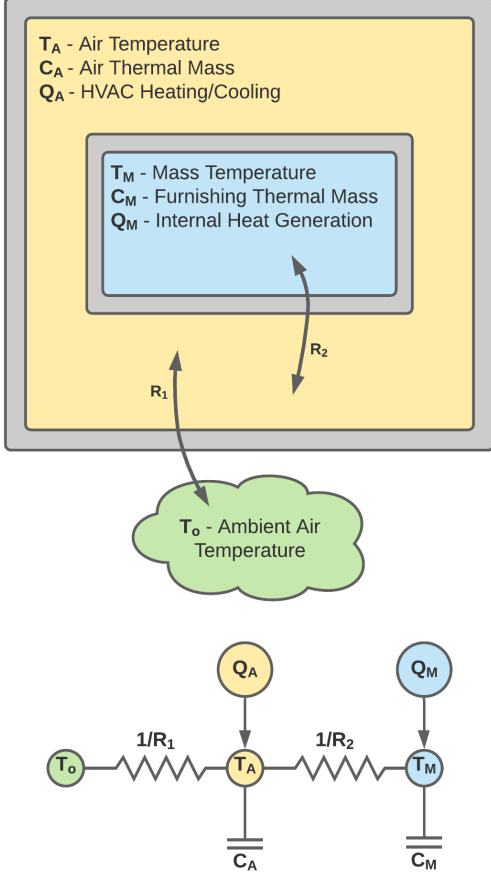


Figure 1: Second-order equivalent thermal parameter circuit diagram.

ature of a home. Using this thermal model, a SSHP's discrete control action may be determined, as will be shown in Section 3.

2.1. Dynamics

Based on the thermal circuit shown in Figure 1, a set of coupled first order differential equations, of the form $\dot{T}_A = f(T_A, T_M, Q_A, T_o, \theta)$ and $\dot{T}_M = f(Q_M, T_A, T_M, \theta)$, are formulated as,

$$C_A \dot{T}_A = Q_A - \frac{1}{R_1} (T_A - T_o) - \frac{1}{R_2} (T_A - T_M), \quad (1)$$

and,

$$C_M \dot{T}_M = Q_M + \frac{1}{R_2} (T_A - T_M). \quad (2)$$

Following [23], Equations (1) and (2) are manipulated to form a second order differential equation in terms of

T_A and its derivatives.

$$\begin{aligned} C_M C_A R_2 \ddot{T}_A + \left(C_M \left(\frac{R_2}{R_1} + 1 \right) + C_A \right) \dot{T}_A + \frac{1}{R_1} T_A \\ = \frac{C_M R_2}{R_1} \dot{T}_o + \frac{1}{R_1} T_o + \eta m. \end{aligned} \quad (3)$$

For ease of representation, the control input, Q_A is replaced with ηm . The term $\eta \in \mathbb{R}$ represents the heat removal capacity of a home's HVAC system, and m scales η according to the output of the governing control algorithm. As it relates to user comfort, a properly functioning control algorithm should modulate the TCL such that a home's temperature T_A is maintained within a prescribed dead-band region $\delta^- \leq T_A \leq \delta^+$. The term Q_M in Equation (2) represents a lumped quantity of internal heat generating elements. Such elements include, but are not limited to, solar radiation, home appliances, and the conductive heat transfer between the home's lumped mass and the ground. This study opts to neglect Q_M based on its relatively small effect when compared to Q_A and heat exchanged with the environment.

The coefficients of Equation (3) are further abbreviated by redefining them as the elements of a parameter vector $\theta \in \mathbb{R}^4$.

$$\theta_1 \ddot{T}_A + \theta_2 \dot{T}_A + \theta_3 T_A = \theta_4 \dot{T}_o + \theta_5 T_o + \eta m \quad (4)$$

As shown in Figure 1, both the outside temperature T_o and its derivative \dot{T}_o represent disturbances to the thermal system. Due to modern meteorological forecasting techniques, it is reasonable to assume that the controller, described in Section 3, has access to future outside temperature data with sufficient accuracy to estimate the control action over a time horizon of a few hours.

This study is dedicated to the optimal control of a population of single speed heat pumps (SSHPs). In the United States, the majority of residential HVAC compressors are governed by the control sequence,

$$m(t) = \begin{cases} 0, & \text{if } T_A \leq \delta^- \\ 1, & \text{if } T_A \geq \delta^+ \\ m(t - \epsilon), & \text{otherwise.} \end{cases} \quad (5)$$

In Equation (5), δ^- and δ^+ represent the lower and upper dead-band thresholds, which T_A cycles between. Symbolically, ϵ represents a finite time shift to a previously known value of m . Based on Equation (5), it is observed that the control action, m , for a SSHP is either 0 or 1 and is a function of the homes air temperature T_A relative to its respective dead-band values. The control action may be mathematically expressed as a binary set $m \in \{0, 1\}$.

Using state space notation, Equation (4) is further restructured as,

$$\dot{\mathbf{x}} = A\mathbf{x} + B(\eta m + \theta_4 \dot{T}_o + \theta_3 T_o), \quad (6)$$

where $\mathbf{x} = [T_A \quad \dot{T}_A]^\top$ and,

$$A = \begin{bmatrix} 0 & 1 \\ -\frac{\theta_3}{\theta_1} & -\frac{\theta_2}{\theta_1} \end{bmatrix}, \quad B = \begin{bmatrix} 0 \\ \frac{1}{\theta_1} \end{bmatrix}.$$

In order to use the model dynamics of Equation (6) in the controller proposed in section 3, this state space representation is first discretized using forward Euler method.

$$\begin{aligned} \mathbf{x}^{k+1} &= (I + \Delta t A) \mathbf{x}^k \\ &+ \Delta t B (\eta m^k + \theta_4 \dot{T}_o(t_k) + \theta_3 T_o(t_k)) \end{aligned} \quad (7)$$

As will be further discussed in Section 3, two indices are used to denote time, namely k and i_k . Of the two indices, k denotes the current time-step of the algorithm, while i_k represents the time-step of the controller's simulation horizon beginning at the k^{th} time-step. Similarly, simulation times may be expressed as,

$$t_k = \Delta t k, \quad (8)$$

and,

$$t_{i_k} = \Delta t(k + i) \in \mathbb{R} \quad \forall i \in \underline{H}, \quad (9)$$

where $\underline{H} = \{1, \dots, H\}$ represents the set of indices over the given simulation horizon.

2.2. Decentralized Network Structure

One of the many goals of this work is to utilize control techniques that result in certain beneficial characteristics of the aggregated power consumption signal defined as,

$$P_{\text{agg}} = \sum_{p \in N} \eta_p m_p. \quad (10)$$

One desired characteristic of a control algorithm is that the peak power consumption of the population of SSHPs be minimized. Another desired characteristic is that the magnitude of the ramp rate of the aggregate power be minimized. As will be shown Sections 3 and 4, these design objectives may be accomplished via peer-to-peer (P2P) communication.

Unlike the top-down command structure of a centralized controller, a decentralized controller relies on localized communication between neighboring TCLs to schedule future control actions. As shown in Figure 2, these SSHPs are represented by the nodes of an unweighted random regular graph.

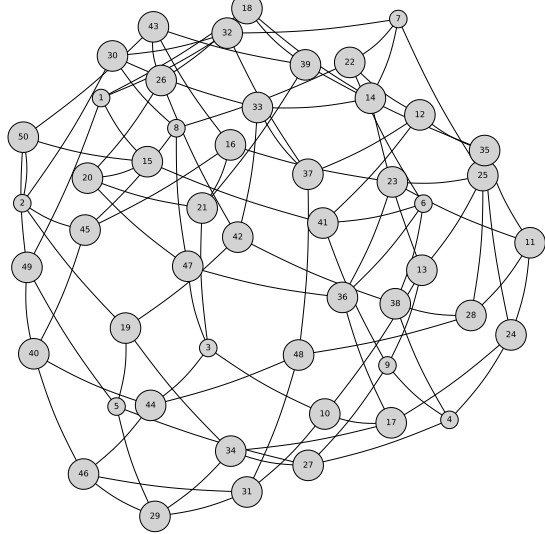


Figure 2: Unweighted random regular graph ($N=50$, $N_{cd} = 4$)

nodes, defined as $\mathcal{N} = \{1, \dots, N\}$, represents the set of all SSHPs in a given population. Communication between two neighboring homes is graphically depicted as an edge between adjacent nodes [4]. Mathematically, an undirected graph, like the random regular graph shown in Figure 2, may be represented by its adjacency matrix, $\mathcal{A} \in \{0, 1\}^{N \times N}$. The $(i, j)^{\text{th}}$ entry of \mathcal{A} is nonzero if node i can communicate with node j .

In this study all connected SSHPs are capable of two-way communication, also referred to as undirected communication. Furthermore, a population of homes is generated such that each SSHP is connected to four neighboring homes. This neighbor set, denoted \mathcal{N}_p , is the list of all TCLs connected to the p^{th} agent. By limiting the number of connections between the p^{th} agent and its neighbor set \mathcal{N}_p to four, communication of sensitive user information is reduced. This information is what might be ascertained if someone were to lower their window and listen to when each neighbors HVAC compressor cycles on or off.

2.3. Lockout Procedure

To ensure the proper operation of a SSHP, further safeguards must exist to prevent the HVAC's compressor from short-cycling. Short-cycling is empirically defined as the rapid cycling of a HVAC system's compressor. Short-cycling has been shown to reduce both the effective lifespan of the compressor and the efficiency of the HVAC system as a whole [24]. HVAC

systems are typically sold in half ton increments, where a ton of cooling is defined as the amount of heat required to freeze/melt two-thousand pounds of water in a twenty-four-hour period. Prior to installation, the tonnage of a HVAC system is chosen according to that home's thermodynamic properties. Characteristics of an oversized HVAC systems is that it toggles on and off quickly, while undersized HVAC systems struggle to maintain temperature during peak cooling hours. To prevent short-cycling, a lockout procedure is incorporated into the controller, which prevents the compressor from cycling on for a brief time period after the compressor turns off. The duration of the lockout period may be heuristically set in accordance to the specifications defined by the HVAC manufacturer.

Similar to how a residential HVAC system is chosen, in this study a HVAC system's cooling capacity $\eta \leq 0$ is determined based on the time required to cool the temperature of a home from the upper dead-band δ^+ to the lower dead-band δ^- . In Figure 1, parameters C_A , C_M , R_1 , and R_2 are initialized based on a predefined mean and standard deviation. By stochastically generating these thermal values, which are used to define the system parameter $\theta^0 \in \mathbb{R}^4$, a population of heterogeneous TCLs may be simulated.

2.4. Parameter Estimation

Elements of the parameter vector θ , which define the model dynamics, are recursively updated in an effort to accurately mimic the dynamics of the plant. Following [25], equation (4) is rewritten as,

$$y_k = \varphi_k^\top \theta_0, \quad (11)$$

where the observed variable y_k and the regressor φ_k are respectively defined as,

$$\begin{aligned} y_k &= \eta m^k, \\ \varphi_k^\top &= [\ddot{T}_A^k \quad \dot{T}_A^k \quad (T_A^k - T_o(t_k)) \quad -\dot{T}_o(t_k)]. \end{aligned} \quad (12)$$

Whether derived from the thermal properties shown in Figure 1, or generated about a known statistical distribution, each element within the initial parameter vector θ_0 needs to be known prior to running the recursive least squares (RLS) algorithm.

$$\theta_0 = [\theta_1^0 \quad \theta_2^0 \quad \theta_3^0 \quad \theta_4^0]^\top \in \mathbb{R}^4, \quad (13)$$

Over a set of initial time-steps $k \in \{1, \dots, k_s\}$, both the observed variables and regressor values are collected to form the following matrices,

$$Y_{k_s} = \begin{bmatrix} y_1 \\ \vdots \\ y_{k_s} \end{bmatrix}, \quad \Phi_{k_s} = \begin{bmatrix} \varphi_1^\top \\ \vdots \\ \varphi_{k_s}^\top \end{bmatrix}. \quad (14)$$

The last time-step $k_s \in \mathbb{N}$ is chosen such that $\Phi_{k_s}^\top \Phi_{k_s}$ is non-singular. Given the initial starting values, θ_0 and $P_{k_s} = (\Phi_{k_s}^\top \Phi_{k_s})^{-1}$, the following RLS algorithm has the following sequence of events,

Algorithm 1 RLS with Exponential Forgetting

- 1: Initialize $P_{k_s} = (\Phi_{k_s}^\top \Phi_{k_s})^{-1}$
 - 2: **while** $k_s < k \leq K$ **do**
 - 3: $S_k = P_{k-1} \varphi_k (\lambda + \varphi_k^\top P_{k-1} \varphi_k)^{-1}$
 - 4: $P_k = (I - S_k \varphi_k^\top) P_{k-1} / \lambda$
 - 5: $\theta_k = \theta_{k-1} + S_k (y_k - \varphi_k^\top \theta_{k-1})$.
 - 6: **end while**
-

In algorithm 1, $\lambda \in \mathbb{R}$ represents the exponential forgetting factor. It should be noted, as $\lambda \rightarrow 1$ the RLS with exponential forgetting becomes the standard RLS algorithm. For various reasons, the thermal parameters of a given home are expected to change over time, therefore inclusion of the exponential forgetting term λ allows for long-term adaptation. Like many other feedback systems, algorithm 1 is subject various amounts of system noise. With the inclusion of a low-pass filter applied to the newly estimated parameters, both system level and measurement noises are damped.

2.5. Demand Response

A major challenge utility service providers face is the implementation of a demand response event, colloquially known as conservation events or peak events. This event, brought forth by the utility service provider, incentivizes or forces its customers to shed power usage during times of peak power consumption. By shedding power, a utility company is able to maintain power generating equipment within safe operating conditions.

For each simulated study shown in Section 4, the following demand response event was implemented. During a time-span t_b , which coincides with the greatest temperature peak $T_{o,max}$, all homes are prevented from conditioning itself. By preventing power consumption over the brief time-span, t_b , a demand response event is generated. Unless power is systematically reinstated, damage to various grid subsystems may occur. The response of the control algorithm to this demand event provides one of the metrics of qualitative performance.

A population of residential homes are simulated under the conventional hysteresis controller (3) to demonstrate the challenges associated with load aggregation.

In this simulation each SSHP control action, m , is governed by Equation (5). As shown in Figure 3b, two types of load aggregation are observed [26, 22, 4]. The first type of load aggregation naturally forms during the morning hours of each day. In a quasi-coordinated fashion, all HVAC systems begin conditioning their respective space leading to spikes in aggregate power consumption. The second type of load aggregation is a result of the demand response event described above. Depending on the duration of this demand response event, each indoor air temperature, T_A , will succinctly rise above its upper dead-band threshold δ^+ . Upon reinstatement of power, these SSHPs begin to condition their respective space resulting in an oscillatory aggregate power consumption signal. This oscillatory ringing continues until the heterogeneous characteristics of the population sufficiently distributes each individual control action. Unless properly damped, this volatile aggregate power consumption has the potential to cause damage to the electric grid.

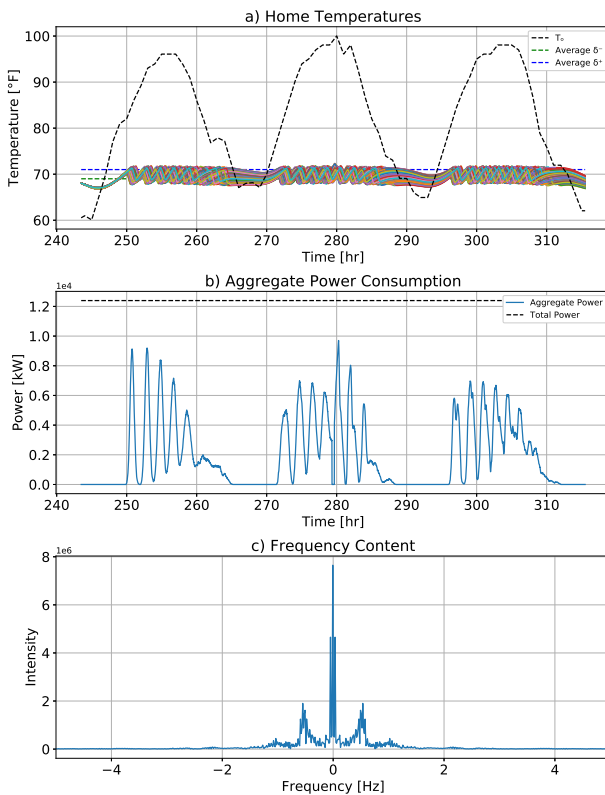


Figure 3: A hysteresis controller, also referred to as a bang-bang control, cycles an HVAC's compressor on and off depending on a home's temperature T_A relative to its proximity to the upper and lower dead-band values denoted δ^+ , and δ^- ($N=1,000$).

3. Controller

For both decentralized and centralized controllers, shown in Sections 3.1 and 3.2, a SSHP's control action m^k , at time k , is generated via model predictive control (MPC). Typically, a MPC calculates the optimal trajectory over a finite time horizon H , which satisfies both the model dynamics and user specifications. Once calculated, the algorithm broadcasts the first control action m^k to the plant. Assuming the system is observable, the measured/predicted states are returned to the controller and are thereby assigned as the initial conditions for the subsequent iteration. The cycle is then repeated until a termination condition is met. This sequence of events is graphically depicted by the system diagram of Figure 4.

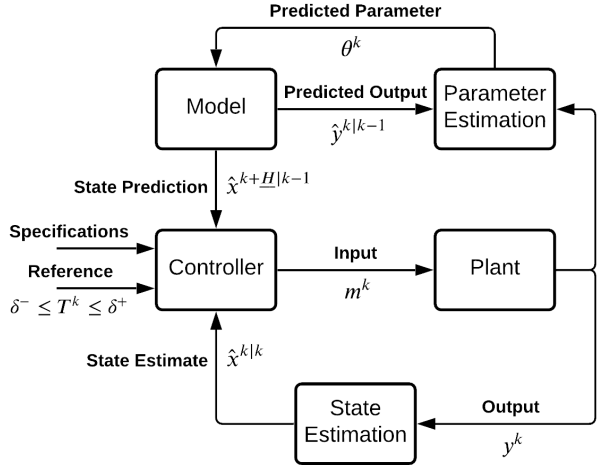


Figure 4: System Diagram.

With regard to the minimization of aggregate power consumption and load volatility, two controllers are presented which schedule the control actions of a population of SSHPs. For the first controller, a decentralized framework is proposed which determines a SSHP's control action based on its neighbor set $m_p^k = \pi(\mathcal{N}_p)$. Similarly, the second proposed controller uses a centralized framework to determine the control action of a population of SSHPs. This centralized framework has complete knowledge of the states and inputs of all SSHPs and is controlled as such $\mathbf{M}^k = \pi(\mathcal{N})$, where $\mathbf{M}^k = [m_1^k, \dots, m_N^k]^T$.

Differences in computational complexity between both decentralized and centralized controllers becomes apparent when performing large scale simulations. For the decentralized discrete controller described in Section 3.1, a mixed integer quadratic program (MIQP) is tasked with solving the control actions, $m^{i_k} \forall i_k \in \underline{H}$, for

a SSHP. Each TCL in this decentralized framework is responsible for calculating its own control action. Unlike this decentralized framework, the proposed centralized controller must determine the control actions for the entire population of TCLs. As a result, the computational complexity for the following decentralized discrete controller remains constant, however, when the population of TCLs grows larger the centralized controller's MIQP becomes computationally intractable.

3.1. Decentralized Discrete Controller (DD)

Using the decentralized control framework described in Section 2.2, an optimal scheduling of control actions over a time horizon \underline{H} is accomplished via the minimization of a properly structured objective function of the state and control variables. This optimization program is defined as the following mixed integer quadratic program (MIQP),

$$\begin{aligned} \min_{\mathbf{x}, m} \quad & J(k, \mathcal{X}_o) = \sum_{i_k \in \underline{H}} \ell_{DD}(i_k, \mathbf{x}^{i_k}, m^{i_k}) \\ \text{s.t.} \quad & \mathbf{x}^0 = \mathcal{X}_o, \\ & \mathbf{x}^{i_k+1} = f_{DD}(i_k, \mathbf{x}^{i_k}, m^{i_k}, \theta^k), \\ & m^{i_k} \in \{0, 1\}, \\ & \forall i_k \in \underline{H}, \end{aligned} \quad (15)$$

where the objective penalty function $\ell_{DD}(\cdot)$ is defined as,

$$\begin{aligned} \ell_{DD}(i_k, \mathbf{x}^{i_k}, m^{i_k}) = -\alpha \left(m^{i_k} - \frac{\sum_{j \in \mathcal{N}_p} m_j^{i_k}}{|\mathcal{N}_p|} \right)^2 \\ -\beta \eta m^{i_k} + \gamma \tilde{T}^{i_k} + \zeta (\dot{T}_A^{i_k})^2. \end{aligned} \quad (16)$$

Expressing the model dynamics of Equation (7) as a set of linear constraints allows the optimizer of Equation (15) to systematically integrate state values over the given simulation horizon \underline{H} , thereby satisfying the dynamics. This set of linear constraints, $f_{DD}(\cdot)$, is expressed as,

$$\begin{aligned} f_{DD}(i_k, \mathbf{x}^{i_k}, m^{i_k}, \theta^k) = (I + \Delta t A) \mathbf{x}^{i_k} \\ + \Delta t B (\eta m^{i_k} + \theta_4 \dot{T}_o(t_{i_k}) + \theta_3 T_o(t_{i_k})). \end{aligned} \quad (17)$$

As previously stated in Section 2.1, \mathbf{x}^{i_k} and m^{i_k} represents the temperature states and control input over a given simulation horizon \underline{H} . The initial condition, denoted \mathcal{X}_o , is systematically assigned by the controller as the plant's estimated response to the control input.

Optimal temperature control is accomplished by minimizing the scalar objective function shown in Equation

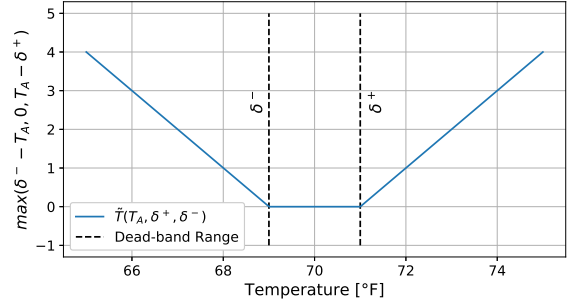


Figure 5: Objective soft constraint \tilde{T} calculated using double hinge function.

(16). By varying \mathbf{x} and m , such that the program's constraints are satisfied, a solution may be realized which is beneficial to both the utility service provider and end-users alike. Based on both utility-provider and end-user requirements, each term in objective function is linked to a particular attribute. These objective terms systematically schedule the control actions of a TCL with regard to its neighbor set \mathcal{N}_p , minimize individual power consumption, maintain a home's temperature within a prescribed dead-band region, and lastly minimize the ramp rate of indoor air temperature.

For the systematic scheduling of control actions, a partial cost is accrued when neighboring SSHPs have a similar control state m^{i_k} . The optimization program minimizes this objective cost by maximizing difference between the p^{th} control input and the average control input of its neighbor set \mathcal{N}_p . Reduction in power consumption occurs with the minimization of the term $-\beta(\eta m^{i_k})$. By convention $\eta \leq 0$, the summation of the objective term $\sum_{i_k \in \underline{H}} -\beta(\eta m^{i_k}) \geq 0$. Indoor air temperature is maintained between its dead-band thresholds by means of a double-hinge soft constraint denoted \tilde{T}^{i_k} . An objective cost is partially accrued when the indoor air temperature rises above δ^+ and falls below δ^- . This soft constraint is defined as $\tilde{T}^{i_k} = \max(\delta^- - T_A^{i_k}, 0, T_A^{i_k} - \delta^+)$ whose graphical representation is shown in Figure 5. Lastly, the quadratic term in the objective function $\zeta(\dot{T}_A^{i_k})^2$ accrues a cost when $|\dot{T}_A^{i_k}| > 0$. Through its minimization, attenuation of the temperature rate of change $\dot{T}_A^{i_k} \forall i_k \in \underline{H}$ is achieved.

Each of the four objective terms are accompanied by an objective constant denoted $\alpha, \beta, \gamma, \zeta \in \mathbb{R}_{\geq 0}$. These positive constants are responsible for scaling the cost of their respective objective term. By altering these objective constants, similar to knobs on a dial, performance of the optimizer may be tuned in accordance to user defined preferences and power consumption restrictions.

The relative magnitude between objective constants determines the controller's response.

3.2. Centralized Discrete Controller (CD)

The following centralized discrete controller provides a baseline of comparison for its decentralized variant. By means of its omniscience, this optimal centralized controller represents a theoretical gold standard. In practice, however, like many other centralized control algorithms, it is burdened with the computational complexity of its population. Similar to the decentralized controller defined by the objective program (16), this centralized controller begins with the definition of its governing optimization program,

$$\begin{aligned} \min_{\mathbf{X}, \mathbf{M}} \quad & J(k, \mathcal{X}_o) = \sum_{i_k \in \underline{H}} g_{CD}(i_k, \mathbf{M}^{i_k}) + \ell_{CD}(i_k, \mathbf{X}^{i_k}, \mathbf{M}^{i_k}) \\ \text{s.t.} \quad & \mathbf{x}_p^0 = \mathcal{X}_{o,p}, \\ & \mathbf{x}_p^{i_k+1} = f_{CD}(p, i_k, \mathbf{x}_p^{i_k}, m_p^{i_k}, \theta_p^k), \\ & m_p^{i_k} \in \{0, 1\}, \\ & \forall p \in \mathcal{N}, \forall i_k \in \underline{H}, \end{aligned} \quad (18)$$

where $\mathbf{X}^{i_k} = [\mathbf{x}_1^{i_k \top}, \dots, \mathbf{x}_N^{i_k \top}]^\top$ and $\mathbf{M}^{i_k} = [m_1^{i_k}, \dots, m_N^{i_k}]^\top$ denote the population of state variables and control inputs at the i_k^{th} time-step. The term $\mathcal{X}_{o,p}$ represents the initial state conditions for the p^{th} home. Within the optimization objective $J(\cdot)$, the function $\ell_{CD}(\cdot)$ is defined as,

$$\ell_{CD}(i_k, \mathbf{X}^{i_k}, \mathbf{M}^{i_k}) = \sum_{p \in \mathcal{N}} -\beta \eta m_p^{i_k} + \gamma \tilde{T}_p^{i_k} + \zeta (\dot{T}_{A,p}^{i_k})^2, \quad (19)$$

and $g_{CD}(\cdot)$, the specialized scheduling term, is expressed as,

$$g_{CD}(i_k, \mathbf{M}^{i_k}) = \alpha \sum_{z=0}^{z_m} \left(\xi^{(z)} \left| \sum_{p \in \mathcal{N}} (m_p^{i_k-z} - m_p^{i_k-z-1}) \right| \right) \quad (20)$$

where $\xi \in \{0, 1\}$ scales subsequent aggregate power difference terms, and $z \in \{0, \dots, z_m\}$ denotes a particular element of the trailing decremented window. For clarity, ξ is raised to the z^{th} power. Equation (20), the objective scheduling term, will accrue a cost if the aggregate control effort, defined by Equation (10), varies between time-steps i_k . Minimizing Equation (20), result is a smoothing effect in the aggregate power consumption signal.

As shown by the objective program (18), each home must satisfy its own dynamic model constraints over the given time horizon \underline{H} . The model dynamics $f_{CD}(\cdot)$ is

Algorithm 2 Decentralized MPC Sequence

```

Initialize  $\mathcal{P} \leftarrow \emptyset, \mathcal{D} \leftarrow \emptyset$ 
 $\mathcal{P} \leftarrow \text{Generate } \theta_0$ 
 $\mathcal{D} \leftarrow \text{Set Initial Conditions}$ 
for  $k = 1$  to  $K$  do
    for  $p = 1$  to  $N$  do
         $m_p^{i_k \in \underline{H}} \leftarrow \text{Controller}(\mathcal{D}, \mathcal{P}, k, p)$ 
         $x_p^k \leftarrow \text{Plant}(\mathcal{D}, \mathcal{P}, k, p, m_p^k)$ 
         $\mathcal{D} \leftarrow x_p^k, m_p^{i_k \in \underline{H}}$ 
    end for
    if  $k \geq 2$  then
         $\mathcal{D} \leftarrow \text{Lockout}(\mathcal{D})$ 
         $\mathcal{P} \leftarrow \text{Algorithm (1)}$ 
    end if
end for

```

similar to that of Equation (17), except now $f_{CD}(\cdot)$ is an explicit function of the p^{th} home.

In reality, the set of control actions, \mathbf{M} , are computed by the optimizer then broadcasted by the utility service provider to their respective HVAC system. Implicitly, there must exist a communication protocol between a utility service provider and its customer to receive state information and thereby transmit the computed control signals. Several methods exist that are capable of sending this necessary bitwise information [27], which is not further discussed.

4. Case Study

Each of the four thermal parameters C_A , C_M , R_1 , and R_2 , which define the controller's model dynamics, are generated about a normal distribution prior to simulation. The specific mean and variance values used to generate the corresponding normal distributions are presented in Table A.2.

With regard to the following simulations, outside temperature, $T_o(t_k)$, is queried from a regional Typical Meteorological Year (TMY) dataset constructed by the National Solar Radiation Database (NSRDB) [28]. Amongst other qualitative properties, this TMY dataset contains ambient outside temperature data sampled at an hourly rate. As the name suggests, a TMY dataset represents the most usual weather conditions for a given region. In this study, a characteristically warm July summers day is simulated to test the performance of the governing controller under strenuous temperature conditions.

By way of algorithm (2), a population of decentralized SSHPs are simulated. At each time-step, k , and

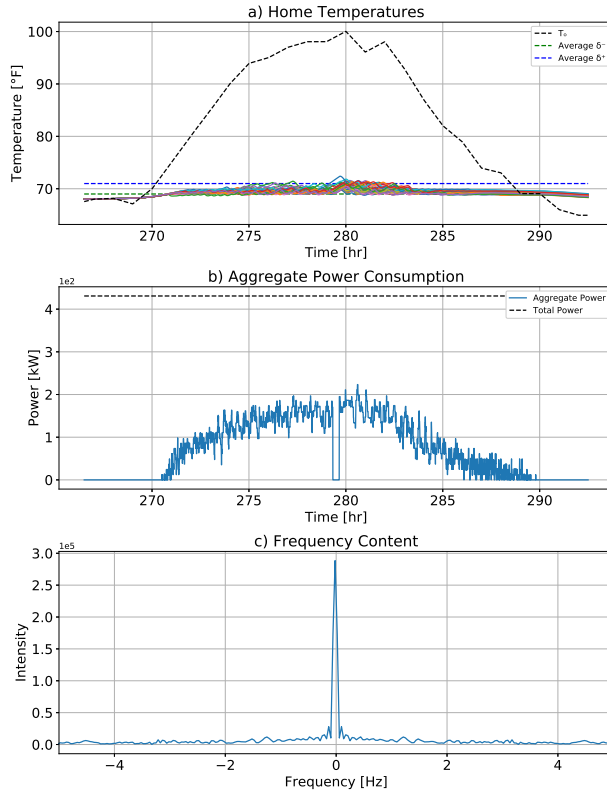


Figure 6: Decentralized discrete controller simulation results ($N=35$).

Table 1: Simulation results.

Simulation Results			
Controller Type	(HC)	(DD)	(CD)
Runtime [sec]	9	961	366
$P\%$	78.3 %	51.8 %	49.2 %
t_{dev} [hr]	2834.8	12.3	125.5

SSHP, p , a horizon of control actions are calculated via the mathematicla program (15). Similarly, a centralized framework, is simulated using the control algorithm (3). In this case, at time-step, k , the mathematical program (18) determines the control actions, $\mathbf{M}^{t_k \in \mathbb{H}}$ for a population of SSHP, \mathcal{N} .

4.1. Comparison

Three qualitative metrics of performance are introduced in this section. These metrics help compare the simulation results generated via algorithms (2) and (3). The first metric of performance, denoted t_{dev} , is a measurement of the cumulative time a population spends above its upper dead-band threshold, δ^+ . Two additional metrics of performance are introduced to compare the aggregate power consumption subplots of Figures 6b

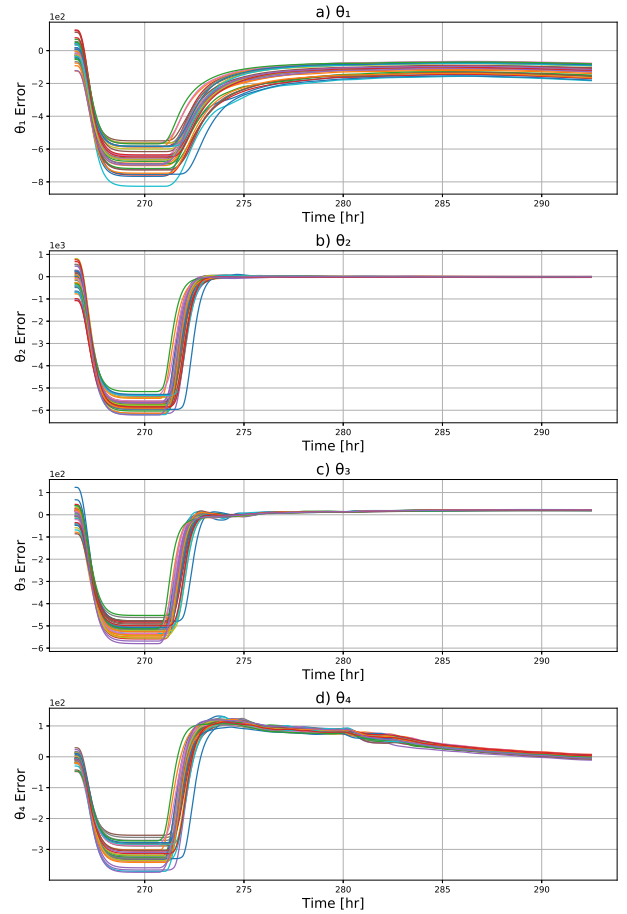


Figure 7: Decentralized discrete parameter estimation results ($N=35$).

and 8b. The first metric, denoted $P\%$, is a ratio between the maximum power consumed and the total expendable power available. Lastly, the third metric is an application of the fast Fourier transform (FFT) on the aggregate power consumption signals. An FFT decomposes a time-domain signal into its corresponding frequency domain. A one-to-one representation of the amplitude of the original signal at each frequency is then plotted to generate Figures 6c and 8c. If the FFT plot has large peaks at a frequency away from zero, we conclude that repeated load synchronization, at this frequency, can be observed in the original signal. The results of $P\%$ and t_{dev} are listed table 1.

In contrast to Figure 3b, both optimal control frameworks significantly reduce the load aggregation induced by the demand response event. This claim is further exemplified by lack of auxiliary peaks in the frequency content subplots of Figures 6c and 8c. Both control frameworks, DD and CD, have similar power ratios, $P\%$, and temperature deviation times t_{dev} . However,

Algorithm 3 Centralized MPC Sequence

```

Initialize  $\mathcal{P} \leftarrow \emptyset, \mathcal{D} \leftarrow \emptyset$ 
 $\mathcal{P} \leftarrow \text{Generate } \theta_0$ 
 $\mathcal{D} \leftarrow \text{Set Initial Conditions}$ 
for  $k = 1$  to  $K$  do
     $\mathbf{M}_{i_k \in \mathcal{H}}^{i_k} \leftarrow \text{Controller}(\mathcal{D}, \mathcal{P}, k, p)$ 
     $\mathbf{X}^k \leftarrow \text{Plant}(\mathcal{D}, \mathcal{P}, k, p, \mathbf{M}^k)$ 
     $\mathcal{D} \leftarrow \mathbf{X}^k, \mathbf{M}_{i_k \in \mathcal{H}}^{i_k}$ 
    if  $k \geq 2$  then
         $\mathcal{D} \leftarrow \text{Lockout}(\mathcal{D})$ 
         $\mathcal{P} \leftarrow \text{Algorithm (1)}$ 
    end if
end for

```

the main feature that sets these two control frameworks apart is the difference in scalability. Both controllers are designed to minimize an objective function over their state and control decision variables. With the centralized framework, the number of decision variables increases linearly with the number of SSHPs being simulated. Since part of these decision variables are integer-valued, they tend to increase the complexity of the optimization problem considerably. As the population size grows, so too increases the computational complexity of the optimization program. Alternatively, the proposed decentralized framework has a fixed number of decision variables thereby maintaining the computational complexity of the mathematical program.

In addition to the tunable objective parameters α, β, γ , and ζ , the centralized framework introduces a trailing window feature, of length $z_m \in \mathbb{N}$, whose terms are increasingly decayed by an amount $\xi \in \mathbb{R}$, shown in Equation (20). Both control frameworks require the judicious selection of each objective constant term. These objective constants, listed in table A.3, were selected in such a way that the conflicting temperature and aggregate power design constraints were balanced. During the selection process of objective constants, the terms z_m and ξ , showed increased levels of sensitivity. Often, the over-abundance of either term resulted in undesirable aggregate power consumption characteristics.

By means of algorithm 1, elements of the thermal parameter vector, θ^k , are recursively updated such that the controller's model dynamics eventually mimic that of the plants' dynamics. To show convergence between the model and plant dynamics, an error signal, defined as the difference between the plant and model parameters $\theta_p^k - \theta_m^k$, is plotted in Figures 7 and 9. Robustness of the RLS algorithm is further improved with the following update conditions, $\kappa(P^k) \leq c_1$ and $\dot{\theta}^k \leq c_2$. The

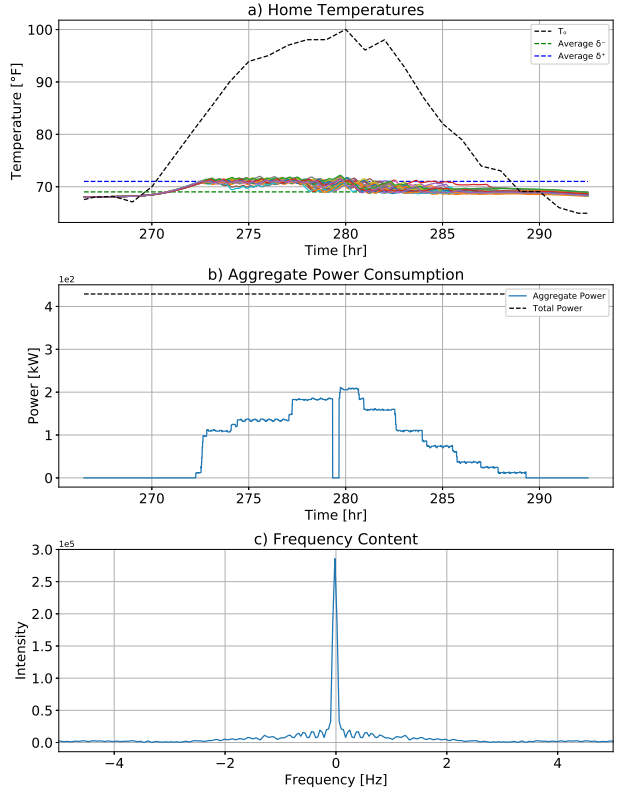


Figure 8: Centralized discrete controller simulation results ($N=35$).

first update condition, $\kappa(P^k) \leq c_1$, requires that the condition number, $\kappa(\cdot)$, of the inverse correlation matrix, P^k defined in algorithm 1, be less than or equal to an empirically determined constant c_1 . The second condition, $\dot{\theta}^k \leq c_2$, requires the rate of change of each model parameter, $\dot{\theta}^k$, be less than or equal to another empirically determined constant, c_2 . The combination of these update conditions, in conjunction a low-pass filter applied to the newly estimated model parameters, was found to improve the robustness and convergence of said parameters. As shown in Figures 7 and 9 (a-d), the model parameters, of both control frameworks, eventually converge upon their corresponding plant parameter. Comparing both figure sets, little to no discernible difference is observed between the convergence properties of each controller.

5. Conclusion

In this paper, we propose a decentralized control framework to aggregate a population of single speed heat pumps in such a way that benefits both the utility service provider and end-users alike. We utilize a second order equivalent thermal parameter model coupled

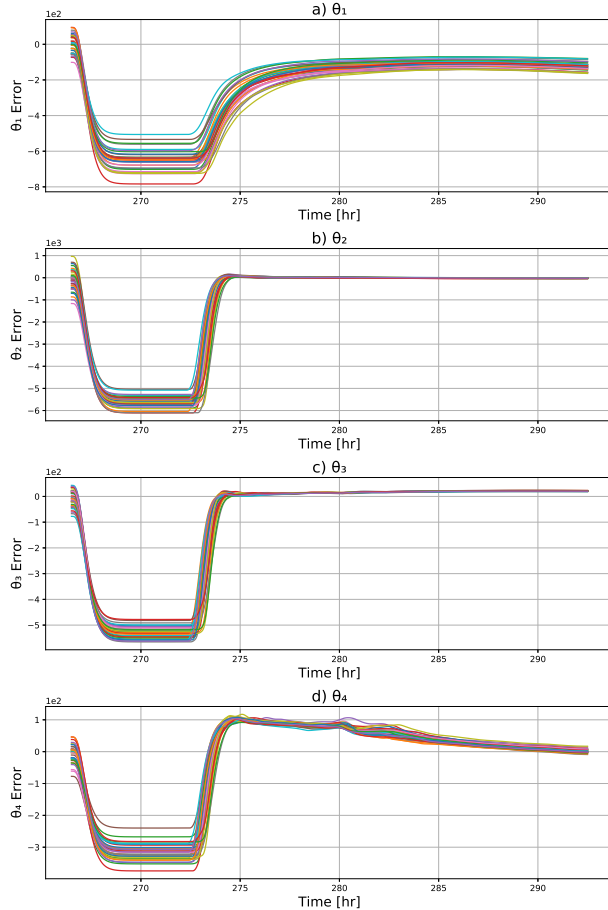


Figure 9: Centralized discrete parameter estimation results ($N=35$).

with a recursive least squares algorithm to accurately model the dynamics of SSHP acting within a residential home. When compared to that of a typical hysteresis controller, we show that the proposed decentralized discrete controller offers a measurable performance increase in metrics of load aggregation and stability. This performance increase is attributed to localized sharing of control actions information which, in turn, allows neighboring SSHPs to infer a near-optimal schedule cycle. For the sake of completeness a centralized control framework is also developed and simulated. This centralized control framework, although not applicable in a physical setting, provides a baseline for comparison with the decentralized framework. Based on our findings, the proposed decentralized controller has comparable attributes to this centralized framework, with the added benefit of its inherent scalability.

References

- [1] H. Hao, B. M. Sanandaji, K. Poolla, T. L. Vincent, A generalized battery model of a collection of thermostatically controlled loads for providing ancillary service, in: 2013 51st Annual Allerton Conference on Communication, Control, and Computing (Allerton), IEEE, 2013, pp. 551–558.
- [2] A. Bacciotti, Stability and Control of Linear Systems, Springer, 2019.
- [3] R. Repice, Monthly energy review (2021). URL <https://www.eia.gov/totalenergy/data/monthly/pdf/mer.pdf>
- [4] J. Kuwada, R. Schwartz, J. F. Gardner, Local communication in populations of thermostatically controlled loads, ASME Journal of Engineering for Sustainable Buildings and Cities 1 (3) (2020).
- [5] R. Malhame, C.-Y. Chong, Electric load model synthesis by diffusion approximation of a high-order hybrid-state stochastic system, IEEE Transactions on Automatic Control 30 (9) (1985) 854–860.
- [6] D. S. Callaway, Tapping the energy storage potential in electric loads to deliver load following and regulation, with application to wind energy, Energy Conversion and Management 50 (5) (2009) 1389–1400.
- [7] W. Zhang, J. Lian, C.-Y. Chang, K. Kalsi, Aggregated modeling and control of air conditioning loads for demand response, IEEE transactions on power systems 28 (4) (2013) 4655–4664.
- [8] S. Koch, J. L. Mathieu, D. S. Callaway, Modeling and control of aggregated heterogeneous thermostatically controlled loads for ancillary services, in: Proc. PSCC, Citeseer, 2011, pp. 1–7.
- [9] M. Liu, Y. Shi, Model predictive control of aggregated heterogeneous second-order thermostatically controlled loads for ancillary services, IEEE transactions on power systems 31 (3) (2015) 1963–1971.
- [10] Y. Zhou, C. Wang, J. Wu, J. Wang, M. Cheng, G. Li, Optimal scheduling of aggregated thermostatically controlled loads with renewable generation in the intraday electricity market, Applied energy 188 (2017) 456–465.
- [11] B. Chen, W. Yao, J. Francis, M. Berges, Learning a distributed control scheme for demand flexibility in thermostatically controlled loads, arXiv preprint arXiv:2007.00791 (2020).
- [12] F. Ruelens, B. J. Claessens, S. Vandael, B. De Schutter, R. Babuška, R. Belmans, Residential demand response of thermostatically controlled loads using batch reinforcement learning, IEEE Transactions on Smart Grid 8 (5) (2016) 2149–2159.
- [13] F. Ruelens, B. J. Claessens, P. Vranckx, F. Spiessens, G. Deconinck, Direct load control of thermostatically controlled loads based on sparse observations using deep reinforcement learning, CSEE Journal of Power and Energy Systems 5 (4) (2019) 423–432.
- [14] H. Kazmi, J. Suykens, A. Balint, J. Driesen, Multi-agent reinforcement learning for modeling and control of thermostatically controlled loads, Applied energy 238 (2019) 1022–1035.
- [15] H. Hao, B. M. Sanandaji, K. Poolla, T. L. Vincent, Aggregate flexibility of thermostatically controlled loads, IEEE Transactions on Power Systems 30 (1) (2014) 189–198.
- [16] D. P. Chassin, J. Stoustrup, P. Agathoklis, N. Djilali, A new thermostat for real-time price demand response: Cost, comfort and energy impacts of discrete-time control without deadband, Applied Energy 155 (2015) 816–825.
- [17] M. Ruth, A. Pratt, M. Lunacek, S. Mittal, H. Wu, W. Jones, Effects of home energy management systems on distribution utilities and feeders under various market structures, Tech. rep., National Renewable Energy Lab.(NREL), Golden, CO (United States) (2015).
- [18] J. Hull, H. Khurana, T. Markham, K. Staggs, Staying in control:

Table A.2: Thermal Parameters.

Thermal Parameter	Mean	Std.
$C_A \left[\frac{\text{Btu}}{\text{°F}} \right]$	1,080	54
$C_M \left[\frac{\text{Btu}}{\text{°F}} \right]$	4,280	214
$\frac{1}{R_1} \left[\frac{\text{Btu}}{\text{°F}\cdot\text{hr}} \right]$	520	26
$\frac{1}{R_2} \left[\frac{\text{Btu}}{\text{°F}\cdot\text{hr}} \right]$	7,050	353

- Cybersecurity and the modern electric grid, IEEE Power and Energy Magazine 10 (1) (2011) 41–48.
- [19] K. Kimani, V. Oduol, K. Langat, Cyber security challenges for iot-based smart grid networks, International Journal of Critical Infrastructure Protection 25 (2019) 36–49.
 - [20] S. H. Tindemans, V. Trovato, G. Strbac, Decentralized control of thermostatic loads for flexible demand response, IEEE Transactions on Control Systems Technology 23 (5) (2015) 1685–1700.
 - [21] Y. Wan, C. Long, R. Deng, G. Wen, X. Yu, T. Huang, Distributed event-based control for thermostatically controlled loads under hybrid cyber attacks, IEEE Transactions on Cybernetics (2020).
 - [22] J. Kuwada, H. Mehrpouyan, J. F. Gardner, Design resilience of demand response systems utilizing locally communicating thermostatically controlled loads, in: ASME International Mechanical Engineering Congress and Exposition, Vol. 59438, American Society of Mechanical Engineers, 2019, p. V006T06A045.
 - [23] J. Fuller, Residential module user's guide (2017). URL http://gridlab-d.shoutwiki.com/wiki/Residential_module_user's_guide
 - [24] S. Ilic, C. Bullard, P. Hrnjak, Effect of shorter compressor on/off cycle times on a/c system performance, Tech. rep., Air Conditioning and Refrigeration Center. College of Engineering (2001).
 - [25] K. J. Åström, B. Wittenmark, Adaptive control, Courier Corporation, 2013.
 - [26] M. S. Nazir, I. A. Hiskens, Load synchronization and sustained oscillations induced by transactive control, in: 2017 IEEE Power & Energy Society General Meeting, IEEE, 2017, pp. 1–5.
 - [27] S. Al-Sarawi, M. Anbar, K. Alieyan, M. Alzubaidi, Internet of things (iot) communication protocols, in: 2017 8th International conference on information technology (ICIT), IEEE, 2017, pp. 685–690.
 - [28] M. Sengupta, Y. Xie, A. Lopez, A. Habte, G. Maclaurin, J. Shelby, The national solar radiation data base (nsrdb), Renewable and Sustainable Energy Reviews 89 (2018) 51–60.

Appendix A. Simulation Parameters

Table A.3: Simulation parameters

	(DD)	(CD)
Objective Constants	α	300
	β	1e-3
	γ	5,000
	ζ	1e-2
	ξ	-
	z_m	10
Simulation Parameters	Homes (N)	35
	Time-step (K)	4,000
	Horizon (H)	20
	Step-length (Δt)	23.4 [sec]
	D.R. Period	20 [min]
	Lockout Period	15 [min]

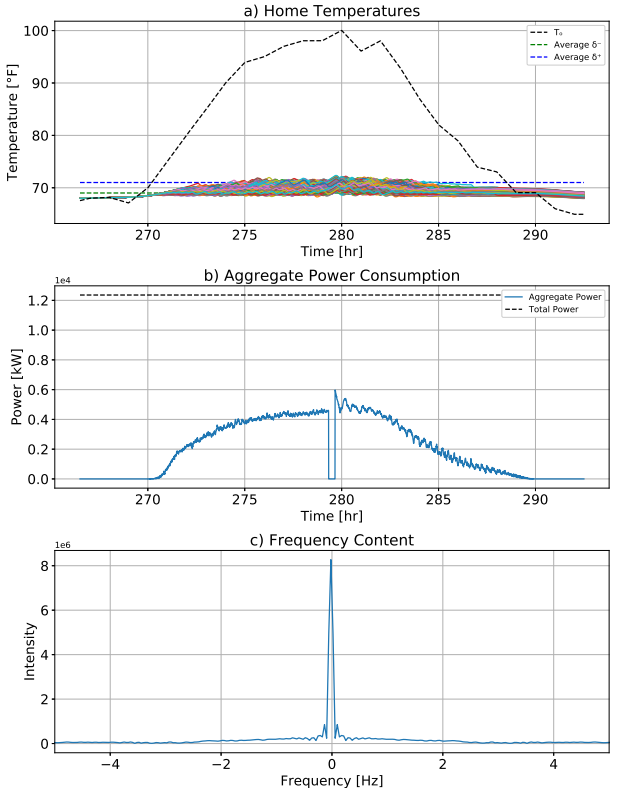


Figure A.10: Decentralized discrete controller simulation results (Runtime 28,331 Seconds, $N = 1000$, $t_{dev} = 396.8$, $P\% = 48.4\%$).

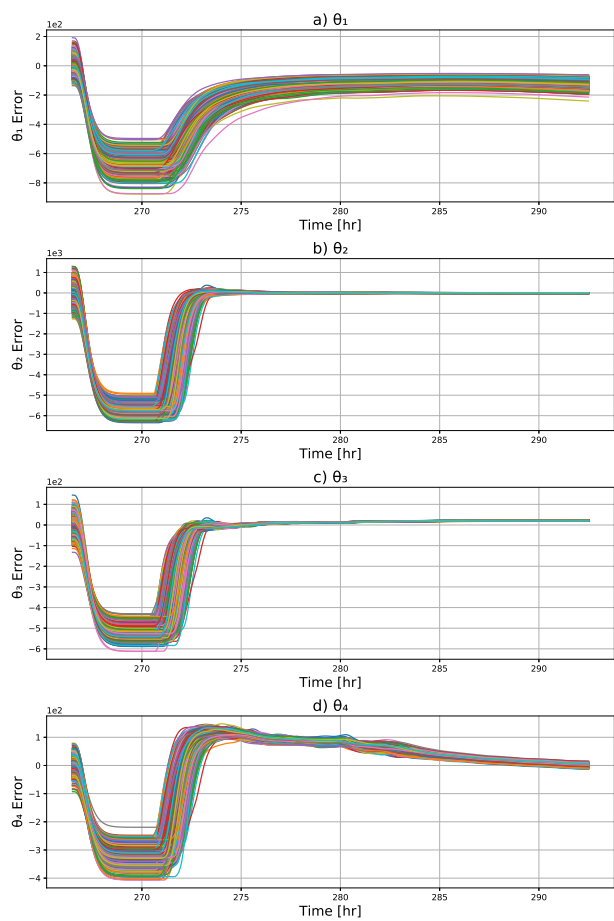


Figure A.11: Decentralized discrete parameter estimation results ($N=1000$).